Phys Chem Minerals (2001) 28: 365–376

ORIGNAL PAPER

K. Kihara

Molecular dynamics interpretation of structural changes in quartz

Received: 17 July 2000 / Accepted: 13 January 2001

Abstract Constant temperature and constant pressure molecular dynamics (MD) simulations were applied to quartz to calculate the structural details which are indeterminable in usual X-ray structure studies. The dynamics of the structural changes was analyzed by means of time-dependent atomic displacement parameters. The Si-O bonds expand with increasing temperatures through the α- and β-phases, and atoms vibrate around the α_1- (or α_2-) sites at lower temperatures in the α-phase, and over the energy barriers between the α_1- and the α_2-sites at higher temperatures in the α- and the β-phases. The ratios of time lengths spent by atoms in the α_1- and α_2-sites determine the apparent atomic positions as obtained in usual structure studies of α-quartz. More frequent transfer of atoms over the α_1- and the α_2-sites contributes positively to the thermal expansions, whereas larger amplitudes of vibrations, which carry atoms more distantly and more frequently from the β-sites, contribute negatively. The well-known steep thermal expansion in the α-phase is attributed to the additive contribution from the expansions of the Si-O bond lengths, the widening of Si-O-Si angles, and the increase of the atomic transfer-frequency between the α_1- and the α_2-sites. The nearly zero or negative expansion in the β-phase is caused by balancing the negative to the positive effects. The MD crystal transforms to the β-phase via a transitional state, where the α- and β-structures appear alternately with time, or coexist. The slight and continuous expansions observed right after the steep rise(s) of the volume or cell dimensions up to the nearly horizontal curve(s) are attributed to the continuous changes within the transitional state.

Key words Quartz · Thermal expansion · Molecular dynamics simulation

K. Kihara
Department of Earth Sciences, Kanazawa University,
Kanazawa 920-1192, Japan
e-mail: kuniaki@kenroku.kanazawa-u.ac.jp

Introduction

Crystals with quartz (SiO_2) type structure with α–β transition show quite different thermal-expansion behaviors below and above the transition points (Jay 1933; Young 1962; Ackermann and Sorrell 1974; Sorrell et al. 1974; Kosten and Arnold 1980). The rapid thermal expansion in α-quartz has been discussed by many authors in relation to the α–β transition. Young (1962) attributed the expansion to the shifts of atomic equilibrium positions under the two restrictions that the Si-O distance be kept constant and that the shifts take place along the lines joining the Dauphiné twin-related positions, α_1 and α_2. Since then, this static interpretation has dominated the thermal expansion studies of α-quartz, resulting in the development of the rotational model, in which the shifts of atomic equilibrium positions are approximated by the rotational displacements of corner-linked rigid (and nearly regular) SiO_4 tetrahedra around $\langle 100 \rangle_{hex}$, combined with translation along $\langle 100 \rangle_{hex}$. The rotational model has been also used to study dynamic aspects such as the soft modes in the α–β transitions. In fact, many authors since Young (1962) have taken advantage of the simplicity in the rotational model (for instance, Höchli and Scott 1971; Megaw 1973; Grimm and Dorner 1975; Liebau and Böhm 1982, and others).

Megaw (1973) showed that the rotation of rigid SiO_4 tetrahedra around $\langle 100 \rangle_{hex}$ from the high symmetry 222 positions produces a reduction of the lattice in both the **a**- and **c**-directions. However, she had to introduce a homogeneous reduction of tetrahedral size for improving the agreement with the observed changes of the cell dimensions at higher temperatures. Grimm and Dorner (1975) considered a similar model. Taking account of possible distortions of the tetrahedra, they further refined the model such that the mean Si-O distance within the tetrahedron decreases with increasing temperature (or rotational angles decrease), being associated with the increase of the Si-O-Si angle.

The negative expansion coefficient of the tetrahedra in the Megaw's (1973) model appears to be consistent with those of the measured Si-O distances in the structure refinements using Bragg diffraction. Grimm and Dorner (1975) refined the model by employing the coordinates of O atoms in the harmonic structure analyses of β-quartz. However, in a more generalized structure refinement of quartz and berlinite, the T-O bond lengths expand with increasing temperature (Kihara 1990; Muraoka and Kihara 1997). The Si-O bond lengths in cristobalite also increase with increasing temperature in a correlation function analysis of neutron powder-scattering intensities (Dove et al. 1997). According to Downs et al. (1992), almost all of the Si-O bond lengths in nine silicates expand with increasing temperature when corrected for tetrahedral libration using a TLS (translational, librational, and screw modes of motion)-rigid-body thermal analysis. All these suggest that the negative expansion of the Si-O bonds in the usual structure refinements using Bragg diffractions is only apparent.

The probability density function (pdf) of an atom in a harmonic crystal may be unimodal with the mode at the minimum of the harmonic potential well. The mode of pdf for an atom is thus located at the position of its mean in harmonic crystals. On the other hand, if atoms undergo anharmonic thermal vibrations, the means are not necessarily at the modes of pdfs. The thermal vibrations of T-O-T bonds in silicates or silicas are typical examples showing librational motions. In the usual harmonic structure refinements of diffraction data, the mean positions of O atoms in these structures may possibly be determined to be those shifted toward the libration axes, T-T (Willis and Pryor 1975), resulting in smaller T-O bond distances than the real ones. Such shifts are expected to become larger with increasing amplitudes of the librational motions at higher temperatures. Indeed, the atomic coordinates obtained in the harmonic structure analyses of quartz (Kihara 1990) showed the Si-O bond lengths becoming smaller with increasing temperatures: the two symmetrically independent Si-O bond lengths of 1.605(2) and 1.614(2) Å at 298 K are reduced to one symmetrically equivalent bond of 1.588(3) Å in β-quartz. Essentially the same feature has also been observed for berlinite (Muraoka and Kihara 1997). On the other hand, the generalized structure analysis, which employs structure factors expanded in higher order terms, is able to locate the modes of pdf more closely to the real positions, from which we can calculate real bond lengths (Johnson 1970). In the anharmonic refinements of quartz and berlinite involving terms up to the fourth order, the separations between the modes of the pdf for bonded Si and O showed values larger than the corresponding distances in the harmonic refinements at high temperatures: 1.620 Å at 848 K and 1.624 Å at 891 K for quartz (Kihara 1990). However, we have experienced in our previous X-ray studies that the determination of anharmonic pdf is easily subjected to deterioration in the quality or reduction in the number of measured intensity data at high temperatures. The above values referring to the separations for the modes are yet to be established.

There have been a number of reported MD studies of the quartz structure. In the extended system (constant temperature and constant pressure) MD study using nonempirical potential parameters, Tsuneyuki et al. (1990) ascribed the dynamical character of β-quartz to cluster dynamics. Tautz et al. (1991) analyzed quantitatively the origin of the incommensurate phase in the MD calculations with 4096 hexagonal unit cells of quartz at different temperatures in the α- and β-phases. Miyake et al. (1998) conducted controlled temperature and pressure MD and discussed details of the change in crystallographic symmetry during the phase transition, using static structure factors calculated based on atom trajectory data.

In addition to these successful studies, we note that real bond lengths and angles are sometimes inaccessible in the usual structure refinements of real crystals, but accessible in MD simulations. It is, of course, possible to calculate the distances and angles for the mean positions of given atoms in the MD system, which are quantities comparable with atomic distances or bond lengths given in the usual structure refinements.

In the present study, constant-temperature and constant-pressure MD simulations were performed on the quartz structure with the three different MD cells of 150, 810, and 1200 hexagonal cells in the α- and β-phases. The cases for 810 and 1200 cells provided almost the same results for the static quantities examined. The mean positions and the distances between those, and the mean-squares displacements of atoms were first calculated from the trajectory data, and then compared with the corresponding X-ray values in the harmonic refinements of Kihara (1990). Next, the distances for Si-O and O-O pairs and the angles of any two given pairs, which may represent real bond lengths and angles, were calculated from the trajectory data. The trajectories of atoms were also used to calculate time-dependent atomic displacement parameters, defined for the displacements measured from the mid-points of α_1–α_2 lines of the atoms. The characteristic thermal expansion behavior was explained through a combination of dynamical effects represented by the atomic displacement parameters and static effects arising from bond-length expansions. Finally, the structures and their changes are discussed by means of the time series of molar volume or atomic displacement parameters. The structural data appearing in this paper are all from the case for 1200 cells. Since our MD crystal sizes are not large enough even for the largest, we have not considered the incommensurate phase.

Computer simulation

The present MD calculations were conducted using the semi-empirical values of the ionic charges and the energy parameters in a two-body potential energy function of the form

$$E = \sum_{i<j} \frac{q_i q_j}{r_{ij}} + f \sum_{i<j} B_{ij} \exp\left[(A_{ij} - r_{ij})/B_{ij}\right] - \sum_{i>j} C_{ij} r_{ij}^{-6} \quad . \qquad (1)$$

The values of the charges, q, are from Kramer et al. (1991), but the potential parameters, A_{ij}, B_{ij} and C_{ij}, for the Si-O and O-O pairs were obtained by equating the Buckingham type expression of Kramer et al. to expression (1). The quantity f is a standard force of 4.184 kJ Å^{-1} mol^{-1}. All the values used are shown in Table 1. A rectangular cell including 18 atoms (6 Si and 12 O) was chosen as $\mathbf{A}_o = [1, 0, 0]$, $\mathbf{B}_o = [1, 2, 0]$ and $\mathbf{C}_o = [0, 0, 1]$ of the hexagonal unit cell. The extended system method by Nosé (1984) for constant temperature MD in combination with the generalized form of the constant pressure MD of Parrinello and Rahman (1981) was employed.

The Lagrangian of the NPT ensemble involves four additional terms in comparison with the conventional NVE MD; two for kinetic and potential energies associated with a degree of freedom, s, and the remaining two for a kinetic energy associated with the MD cell and a potential energy PV (Nosé 1984; Parrinello and Rahman 1981). Two parameters Q and W, which determine the time scale of temperature fluctuations and the relaxation time for recovery from an imbalance between external pressure and internal stress, respectively, are introduced in the dynamic equations for s and V. It is, however, indicated that static quantities obtained from the trajectory data of the MD are independent of the values chosen for Q and W (see, for instance, Andersen 1980; Parrinello and Rahman 1981; Nosé 1984). Furthermore, some dynamic quantities are believed to be less sensitive to Q (Nosé 1984).

In this study, simulations with more than 20 different combinations of Q and W were first carried out on a ($5\mathbf{A}_o$, $3\mathbf{B}_o$, $5\mathbf{C}_o$) MD cell including 150 hexagonal cells. Then the effects of different MD cell sizes were examined by applying a combination of W and Q to the three different MD cells of 150, 810, and 1200 hexagonal cells, each corresponding to $(5 \times 3 \times 5)$, $(9 \times 5 \times 9)$ and $(10 \times 6 \times 10)$ cells of the ($\mathbf{A}_o$, $\mathbf{B}_o$, $\mathbf{C}_o$) cell. Compared are time-averaged quantities (cell dimensions, atomic coordinates, and mean-squares displacements), and time-dependent quantities (fluctuations of molar volume and atomic displacement parameter defined later). The transition temperature was also compared for the different MD-cell sizes. The simulation for the $(10 \times 6 \times 10)$ cell was most intensively carried out.

A series of the NPT simulations with increasing temperature for the ($10\mathbf{A}_o$, $6\mathbf{B}_o$, $10\mathbf{C}_o$) MD cell were commenced at 300 K: the starting positions of 10 800 atoms were derived from the X-ray coordinates of α-quartz in space group $P3_221$ at room temperature. The values at the final step of a simulation at a temperature were used as the starting values in the next highest temperature calculations: a similar process was repeated at 17 different temperatures up to 1300 K, all under atmospheric pressure. The MD runs were performed with the W and Q values of 500 g mol^{-1} and 100 kJ mol^{-1} (ps)^2, respectively, and with a step width of 1 fs. The first 5000 steps were sufficient to equilibrate the system except for temperatures near the transition point, and the trajectory data at every tenth step of the 40 960 steps of a run after equilibrating were stored for the analyses. The vicinity of the transition point was intensively examined with smaller temperature intervals, 880, 900, 910, 915, 920, 925, 930, and 950 K to find the transition. The time-averaged $\langle s \rangle$ values were confined in narrow ranges from 0.996 to 1.014, with the fluctuations less than 0.009 in the final runs at all temperatures. Averaged temperatures over whole time steps were well controlled within the ranges of about 10^{-5} of set values.

Table 1 Energy parameters and charges used in MD simulations. Charges are from Kramer et al. (1991), but the potential parameters in the Buckingham type expression of these authors are transformed for the use in expression (1)

Pair	C_{ij} (kJ Å^6 mol^{-1})	A_{ij} (Å)	B_{ij} (Å^{-1})	Charge (|e|)
Si-O	12 888.865	2.97960	0.20521	$q_{Si} = +2.4$
O-O	16 890.695	4.12674	0.36232	$q_O = -1.2$

Results and discussion

The most remarkable in the present simulations with different MD cells is the simulated transition temperatures: the case for the $(5 \times 3 \times 5)$ cell provided temperatures as high as 1300 K, much higher than about 910 K for the cases of the $(9 \times 5 \times 9)$ and $(10 \times 6 \times 10)$ cell. The differences between the simulations for the latter two cases, both undertaken with a combination of $W = 500$ g mol^{-1} and $Q = 100$ kJ mol^{-1} (ps)^2, are within statistical uncertainties as far as the time-averaged quantities including the transition temperature are concerned.

On the other hand, in further trial simulations for the $(5 \times 3 \times 5)$ cell, the effects of the different values of W and Q on the transition temperature and the time-averaged quantities were not sensitive. Two cases examined with $W = 100$ g mol^{-1} and $Q = 20$ kJ mol^{-1} (ps)^2, and $W = 500$ g mol^{-1} and $Q = 100$ kJ mol^{-1} (ps)^2 showed almost the same temperature between 1280 and 1300 K. Many runs with the different combinations of W and Q were attempted to find the effect of these values, resulting in nearly equal values for each of the time-averaged quantities. The time scales of the fluctuations of volume and of atomic displacement parameters, however, were weakly affected by different W and Q. The structural data in the present study are all referred to the simulations for the $(10 \times 6 \times 10)$ cell.

Cell dimensions and the transition temperature

The MD cell, averaged over all stored time steps, well maintains the metric relation for the hexagonal lattice. The hexagonal cell dimensions and volume are compared with the X-ray data (Kihara 1990) in Fig. 1 as a function of temperature. The characteristic features in the temperature dependence of the cell dimensions observed in the experiments are well reproduced. The sharp changes at about 900–920 K apparently represent the α–β transition. In the intensive measurements of the cell dimensions around the α–β transition with X-ray or neutron powder diffractions by Carpenter et al. 1998 and Welche et al. 1998, the **a**-dimension continues to increase in the range of about 80 K after the transition point while **c** increases in the range of about 20 K and then begins to decrease. Our MD cell sizes also show similar tendency (Fig. 1c); that is, after the steep increase up to the nearly horizontal curve, **a** keeps a slightly expanding trend in the range of about 300 K, while **c** begins to decline after arriving at the maximum within about 100 K. This weak but characteristic feature around the transition is explained in relation to the emergence of a transitional state later on. The cell volume is about 3% larger than the X-ray data in either the α- (at 300 K) or β-phase.

According to the temperature dependence of the cell constants and atomic fractional coordinates, the $\alpha \rightarrow \beta$

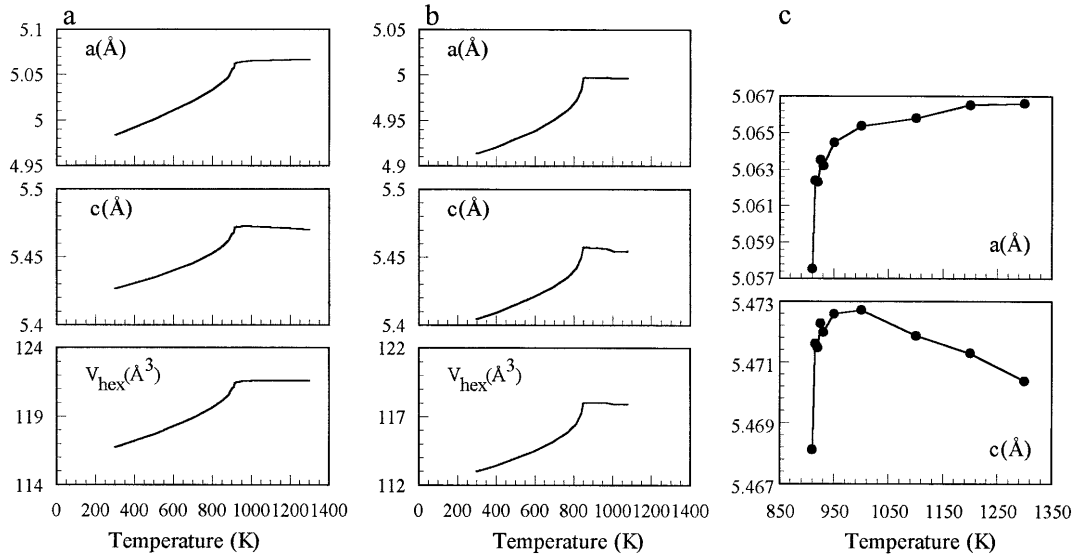

Fig. 1a–c Temperature dependence of hexagonal cell dimensions a and c, and volume V in molecular dynamics simulations in comparison with X-ray results (Kihara 1990). **a** MD. **b** X-ray. **c** Close-up of the a and c dimensions in MD. *Lines* connect hidden data points

transition occurs between 900 and 920 K in the present MD system, which is higher than the observed value of 846 K. In this paper, the temperatures are expressed in the differences from 910 K, if necessary for comparison with the experiments.

Atomic mean positions and mean-squares displacements

One Si and one O atom were selected to represent the asymmetrical unit of the space group of the α-phase, i.e., $P3_221$, and then the atomic coordinates for these atoms were averaged over the whole stored time steps and all the symmetrically equivalent atoms in the $(10 \times 6 \times 10)$ cell. Table 2 shows the atomic coordinates at $\Delta T = -610$ K(300 K) and $+40$ K(950 K) in the fractions of the averaged hexagonal cell, together with the X-ray values in the harmonic refinements at $\Delta T = -548$ K(298 K) and $+45$ K(891 K) (Kihara 1990). The atomic fractional coordinates shift toward the higher symmetry sites, which we refer to as the β-sites, as observed in the X-ray studies of α-quartz. The (averaged) coordinates of Si and O at $\Delta T = -10$ and 0 K are already very close to those of the β-sites, but show slight fluctuations from run to run until $\Delta T = +15$ K: for example, the coordinates of Si at $\Delta T = 0$ K change in the range of $(\pm 0.01, 0, 0)$ around (0.500, 0.000, 0.000). This instability could be related to the long-lived clustered fluctuations of atoms in the transitional state.

The mean-squares displacement matrix for each atom is defined by:

$$\mathbf{B}(\kappa) = \langle \mathbf{u}(\kappa)\mathbf{u}(\kappa)^{\mathrm{T}} \rangle \ , \qquad (2)$$

where $\mathbf{u}(\kappa)$ and $\mathbf{u}(\kappa)^{\mathrm{T}}$ are a 3×1 column matrix and its transpose with elements representing the components of the displacements of atom κ along the Cartesian axis, and the brackets $\langle \cdots \rangle$ indicate an average over all possible displacements (Willis and Pryor 1975). In usual diffraction studies, the temperature factors of an atom are obtained from averaging over symmetrically equivalent atoms. In the present study, all 18 atoms in an ($\mathbf{A}_o$, $\mathbf{B}_o$, $\mathbf{C}_o$) cell were chosen and the averages of Eq. (2) were taken over the whole stored time steps. In order to compare with the X-ray mean-squares displacements,

Table 2 Fractional atomic coordinates in molecular dynamics simulation of α- and β-quartz in comparison with X-ray values

	α-Quartz			β-Quartz		
	$\langle x \rangle$	$\langle y \rangle$	$\langle z \rangle$	$\langle x \rangle$	$\langle y \rangle$	$\langle z \rangle$
Si MD[a]	0.4694	0.0000	0.0000	0.5000	0.0000	0.0000
X-ray[b]	0.4697(1)	0	0	0.5	0	0
O MD[a]	0.4225	0.2654	0.1259	0.4273	0.2136	0.1667
X-ray[b]	0.4133(3)	0.2672(3)	0.1188(2)	0.4155(9)	0.2077	0.1666

[a] MD values at 300 K ($\Delta T = -610$ K) for α-quartz and 950 K ($\Delta T = +40$ K) for β-quartz. ΔT is the temperature measured from 910 K

[b] X-ray values at 298 K ($\Delta T = -548$ K) and 891 K ($\Delta T = +45$ K) (Kihara 1990). ΔT is the temperature measured from the transition point, 846 K. Standard deviations in parentheses are of symmetrically constrained refinements: $\langle y(\mathrm{Si}) \rangle = \langle z(\mathrm{Si}) \rangle = 0$ for α-quartz, and $\langle x(\mathrm{Si}) \rangle = 0.5$, $\langle y(\mathrm{Si}) \rangle = \langle z(\mathrm{Si}) \rangle = 0$, $\langle y(\mathrm{O}) \rangle = \langle x(\mathrm{O}) \rangle / 2$, and $\langle z(\mathrm{O}) \rangle = 1/6$ for β-quartz

averaging was extended to involve all translationally equivalent atoms and then all rotationally equivalent ones. In Table 3, the diagonalized mean-squares displacements for Si and O obtained at $\Delta T = -610$ and $+40$ K are compared with the corresponding X-ray values at $\Delta T = -548$ and $+45$ K, respectively. The calculated **B** matrices for Si and O are both represented by the anisotropic ellipsoids. The agreement between the experiments and the present simulations is surprisingly good in both the magnitudes and the directions of the principal axes (Table 3), except for a couple of points. Axes 2 and 3 for Si in the β-phase are calculated with apparently large deviations from the expected site symmetry, i.e., 222. However, Table 3 also shows that the ellipsoid for Si is almost perfectly spherical in the section perpendicular to $[100]_{hex}$. The apparent violation of the symmetry is thus not as serious as it appears. We note rather a little smaller magnitude in the longest axis of the O ellipsoid than the X-ray ones at all temperatures. Figure 2 shows the temperature dependence of the mean-squares displacements for O and Si atoms in their principal axes in comparison with the corresponding X-ray ones. The axes 1 for both Si and O in the simulation (a and d in Fig. 2) show sharper changes than the others, as observed in the X-ray studies of quartz shown in Fig. 2b (Kihara 1990) or berlinite (Muraoka and Kihara 1997). The thermal vibrations in axes 1 are contributed by low-frequency modes with rotational components of the corner-linked TO_4 units (Kihara 1993). Such important components for small wave vectors are possibly excluded in the present simulations with the limited MD cell size. Simulations with larger MD cells are expected to give larger magnitudes in axes 1.

Similarly to the calculation of $\mathbf{B}(\kappa)$ in Eq. (2), the positions of all translationally equivalent atoms in the MD cell were accumulated to construct the pdf for each of the 18 atoms in the ($\mathbf{A}_o$, $\mathbf{B}_o$, $\mathbf{C}_o$) cell, which was unimodal for every atom even in the β-phase, as shown by the X-ray study (Kihara 1990).

On the basis of the good MD results for the time-averaged quantities, we address the problems which we could not solve directly in our previous diffraction study on quartz.

Atomic distances and angles

The temperature dependence of the separations between the time-averaged atomic positions of bond-forming Si and O atoms, denoted as $\langle$Si$\rangle$-$\langle$O$\rangle$, are compared with those for the X-ray harmonic refinements (Kihara 1990) in Fig. 3. The two independent $\langle$Si$\rangle$-$\langle$O$\rangle$ distances con-

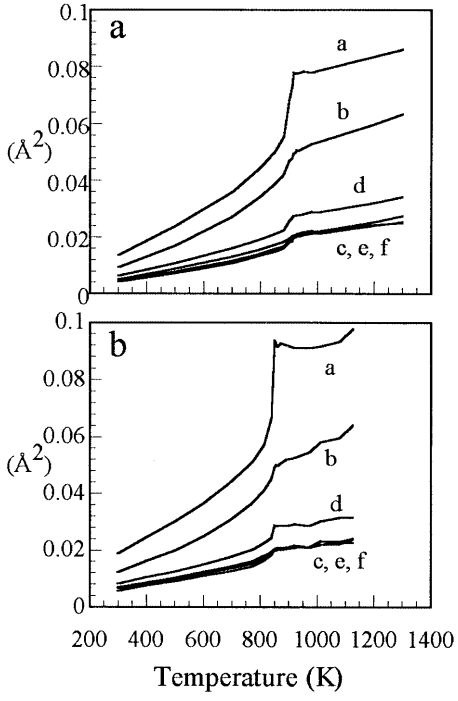

Fig. 2a, b Temperature evolution of mean square displacements of an O atom and a Si atom in the principal axes of $\langle \mathbf{uu}^T \rangle$ ellipsoids in MD in comparison with the X-ray ones. **a** MD. **b** X-ray (Kihara 1990). The first (largest), second, and third axes are marked, respectively, by *a*, *b*, and *c* for O, and by *d*, *e*, and *f* for Si. *Lines* connect hidden data points

Table 3 Atomic mean-squares displacements in principal axes in molecular dynamics simulation of α- and β-quartz in comparison with the X-ray values. Principal axes are expressed in angles (degrees) from [210], [010], and [001] of the hexagonal lattice. For each axis, MD values at 300 K ($\Delta T = -610$ K) and 950 K ($\Delta T = +40$ K) are shown in *upper lines*, and X-ray values at 298 K ($\Delta T = -548$ K) and 891 K ($\Delta T = +45$ K) (Kihara 1990) are in *lower lines* with standard deviations for magnitudes in *parentheses*

	Si				O			
	$\langle u^2 \rangle$ (Å^2)	∧[210]	∧[010]	∧[001]	$\langle u^2 \rangle$ (Å^2)	∧[210]	∧[010]	∧[001]
α-Quartz								
Axis 1	0.0068	31	120	87	0.0136	31	79	117
	0.0082(3)	30	120	90	0.0189(3)	38	72	122
Axis 2	0.0062	99	111	22	0.0101	60	120	44
	0.0070(2)	97	103	15	0.0123(6)	52	118	50
Axis 3	0.0049	61	39	67	0.0055	85	32	58
	0.0058(2)	61	33	75	0.0066(6)	86	34	56
β-Quartz								
Axis 1	0.0283	31	121	90	0.0785	89	139	48
	0.0286(7)	30	120	90	0.0921(2)	90	134	44
Axis 2	0.0218	60	33	76	0.0515	8	96	84
	0.0212(6)	60	30	90	0.0522(2)	0	90	90
Axis 3	0.0212	98	104	16	0.0209	87	44	47
	0.0206(5)	90	90	0	0.0210(2)	90	44	46

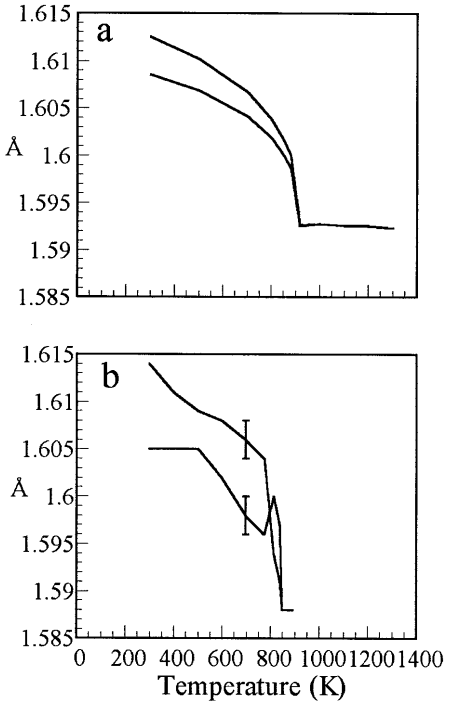

Fig. 3a, b Two independent distances between time- and ensemble-averaged Si and O positions in MD compared with X-ray distances at various temperatures: **a** MD. **b** X-ray harmonic refinement (Kihara 1990). *Lines* connect hidden data points

tinuously decrease from 1.608 and 1.613 Å at $\Delta T = -610$ K to 1.592 Å in the β-phase, where the values remain nearly constant. These values compare well with the corresponding distances in the X-ray study, 1.605(2) and 1.614(2) Å at $\Delta T = -548$ K and 1.588(3) Å in the β-phase. We next show that, in spite of the reduction of ⟨Si⟩-⟨O⟩, the Si-O bonds expand with increasing temperature.

The time-averaged distances for Si-O, O-O, and Si-Si, and angles for Si-O-Si and O-Si-O, all denoted as ⟨Si-O⟩, ⟨O-O⟩, ⟨Si-Si⟩, ⟨Si-O-Si⟩, and ⟨O-Si-O⟩, respectively, are directly calculated from the trajectory data for a given SiO_4 tetrahedron and Si-O-Si bond. As far as we have inspected, there is no significant violation of the space group symmetry of $P3_221$ or $P6_222$ in the time-averaged values for the distances and angles. Figure 4 illustrates the temperature dependence of the values for an arbitrarily chosen SiO_4 tetrahedron and Si-O-Si bond. The root-mean-squares displacements for the lengths and angles for the tetrahedron are about 0.03 and 0.06 Å for Si-O, 0.06 and 0.12 Å for O-O, 6 and 12° for Si-O-Si, and 3 and 6° for O-Si-O at $\Delta T = -610$ K and $+390$ K, respectively. The time-averaged SiO_4 tetrahedra (com-

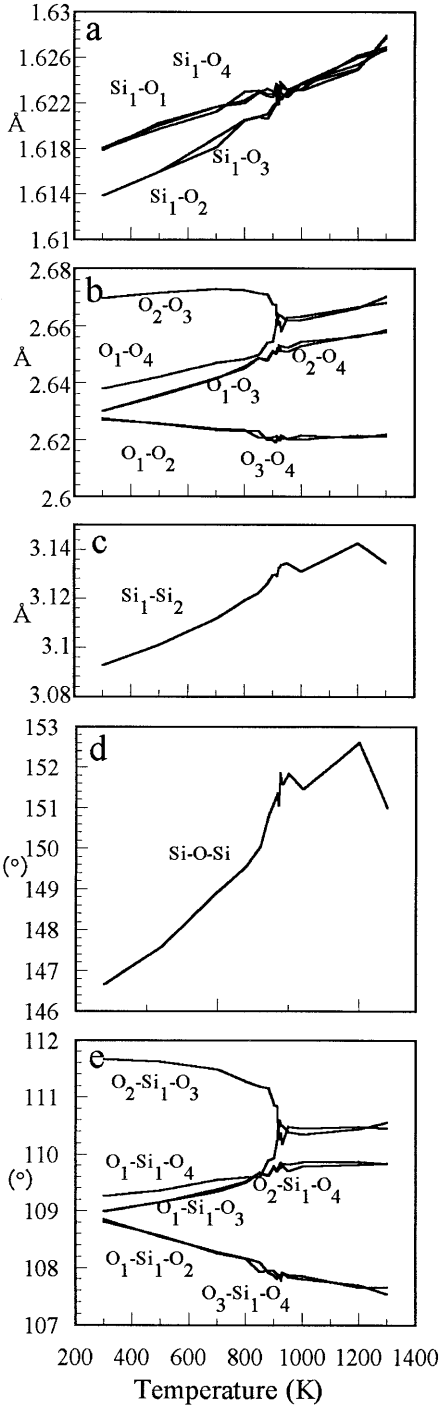

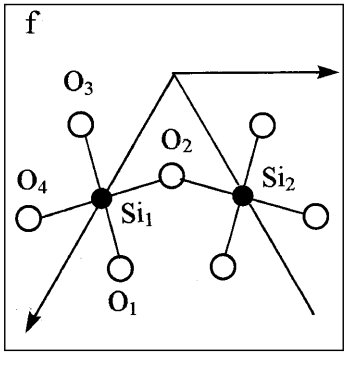

Fig. 4a–f Temperature evolution of time-averaged distances (Å) and angles (°) for atoms in an arbitrarily chosen SiO_4 tetrahedron and a Si atom linked to the tetrahedron. **a** Si-O. **b** O-O. **c** Si-Si. **d** Si-O-Si. **e** O-Si-O. *Lines* connect hidden data points. The positional relation is given in **f**

posed of ⟨Si-O⟩ and ⟨O-O⟩) are distorted in a manner consistent with the space groups of the α- and β-phases from the regular tetrahedron: the distances, ⟨Si-O⟩ and ⟨O-O⟩, and angles ⟨O-Si-O⟩ have two, four, and four different values, respectively, in the α-phase, but one, three, and three values in the β-phase. The two symmetrically independent ⟨Si-O⟩s at $\Delta T = -610$ K are 1.614 and 1.618 Å, which are apparently larger than the X-ray values, 1.605 and 1.614 Å, respectively, in the harmonic refinements at $\Delta T = -548$ K (Kihara 1990). We note that free-energy minimization calculations of De Boer et al. (1996), based on quasiharmonic approximation with the potential energy parameters of Kramer et al. (1991), predicted smaller Si-O distances, 1.598 and 1.606 Å at 300 K, than the present ones and even than the X-ray values. Among the tetrahedral angles, three are centered on 109° and one on 111° at $\Delta T = -610$ K. The three kinds of the tetrahedral angles in the β-phase are about 110.5(×2), 109.8(×2) and 107.6(×2)° at $\Delta T = +390$ K. The Si-O-Si angles widen from about 146.5° at $\Delta T = -610$ K to about 152° in the β-phase.

The two ⟨Si-O⟩ bond lengths continuously expand with increasing temperature: the two curves merge at about $\Delta T = 0$ K, where ⟨Si-O⟩ is 1.622 Å, and then rises almost linearly up to 1.628 Å at $\Delta T = +390$ K. The expansion coefficient of the Si-O bond is about 0.74×10^{-4} K^{-1} in the range from $\Delta T = -610$ K to $+390$ K. It is important to note for the present MD simulations that the bond lengths continuously increase in the β-phase, but the unit-cell dimensions remain almost unchanged with increasing temperature. We will discuss this later.

Atomic displacement parameter and structure changes

According to the structural studies of Young (1962), in which positional parameters are expressed in fractional coordinates, the equilibrium position of an atom at a temperature below the α–β transition is somewhere on the path from the α_1-site (or α_2-site) to the mid point of the α_1- and α_2-sites, i.e., the β-site. The α_1-site is the room temperature equilibrium position of an atom and α_2 its Dauphiné twin-related position. The β-site is essentially invariant with varying temperature, as far as fractional coordinates are concerned. In analyzing the trajectories, we can conveniently express the time-dependent atomic positions by means of displacements from the β-sites. A time-dependent atomic displacement parameter, denoted $\eta(\kappa, t)$, for atom κ, is defined as

$$\eta(\kappa, t) = \frac{d(\kappa, t)}{\delta(\kappa)_{300\mathrm{K}}} \quad ,$$

where $d(\kappa, t)$ is the time-dependent separation of atom κ from its β-site, and $\delta(\kappa)_{300\mathrm{K}}$ the distance between the β-site and α_1-site (or α_2) of atom κ at 300 K, the lowest temperature of the present study. It was found that the histogram of $\eta(\kappa, t)$ for atom κ shows the peak at almost the same η-value as those for different κ's: for example, all examined atoms showed the peaks at $\eta \approx +1$ at 300 K and ≈ 0 for the β-phase. The atomic displacement parameters could be the macroscopic order parameter for the $\alpha \rightarrow \beta$ transition, if they are averaged over time and accumulated for all atoms in the system. The trajectories of an atom are analyzed using $\eta(\kappa, t)$ or the components in the line joining its β- and α-sites, denoted $\eta_{\beta\alpha}(\kappa, t)$.

Although Megaw (1973) and Grimm and Dorner (1975) considered the static interpretation for the thermal expansion in α-quartz, their studies are applicable to the time evolution of the cell size, i.e., the cell size decreases when the rigid tetrahedrons tilt away from the β-sites. The recent study by Welche et al. (1998) indicates that many low-frequency modes with substantial rotational components are associated with negative Grüneisen parameters. All these studies indicate that the thermal expansion in quartz is related to the rotational displacements of the corner-linked SiO_4 tetrahedrons, either static or dynamic. We first analyze the changes of the atomic positions in the α-phase, and then show that the steep expansion in the α-phase is caused by a combination of dynamic and static effects.

Figure 5 shows the time series of $\eta(\kappa, t)$ for an oxygen atom at $\Delta T = -610$, -210, -10, $+90$ and $+390$ K. At lower temperatures in the α-phase, the atom vibrates in the α_1- or α_2-site as shown in Fig. 5a: in other words, the atomic pdf is a well-defined sharp single-peaked distribution with the means at $\eta \approx +1$ (or -1). With increasing temperature, the amplitude of vibration increases, causing the atom to move to the α_2-side. In Fig. 5b, we see that, at $\Delta T = -210$ K, the atom that has moved to the side of the α_2-site quickly returns to the α_1-site. At $\Delta T = -10$ K (Fig. 5c), the atom oscillates

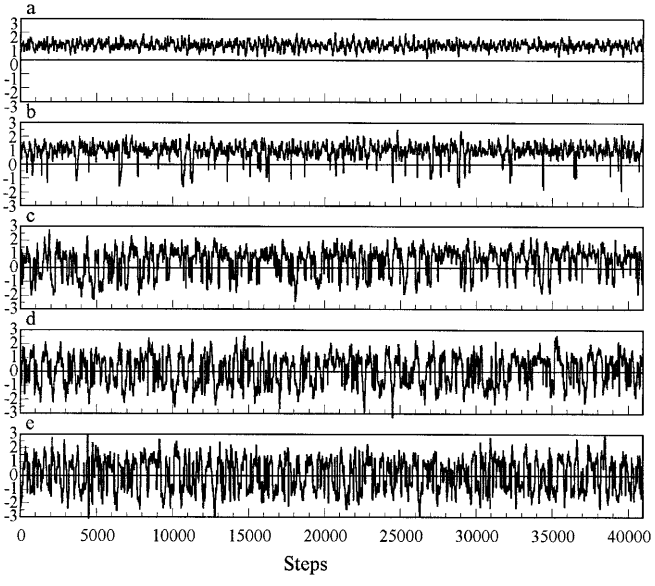

Fig. 5a–e Time series of displacement parameters, $\eta(\kappa, t)$ for an O atom at an every tenth step of 40 960 steps at five temperatures, **a** $\Delta T = -610$, **b** -210, **c** -10, **d** $+90$, **e** $+390$ K. Temperatures for MD are expressed in differences from 910 K

over the boundaries between the α_1- and α_2-sites, spending consecutive time steps in the α_1-site for about 200–1000 steps and then in the α_2-site for about 200 steps at the maximum. In the β-phase (Fig. 5d, e), the atom oscillates in the α_1-site ($\eta = +1$) for 200–300 steps (0.2–0.3 ps) and then moves to the α_2-site ($\eta = -1$) to oscillate for approximately the same time steps as for the α_1-site, resulting in a large total amplitude of thermal vibration as illustrated in Fig. 2. The behavior, involving time scales presented above about the displacement parameters for an O atom, was found to be common to the remaining O and Si atoms as far as we examined.

According to the observations with $\eta(\kappa, t)$ or $\eta_{\beta\alpha}(\kappa, t)$, the mean positions of atoms are determined by the ratios of the time lengths spent by the atoms in the α_1- and α_2-sites. The higher symmetry, $P6_222$, of the β-phase is attained for atoms spending time evenly at the two sites.

Thermal expansions and displacement parameter

If the Fourier transforms of a pair of random processes, $x(t)$ and $y(t)$, are given as

$$X(\omega) = \frac{1}{2\pi} \int_{-\infty}^{\infty} x(t) \exp[-i\omega t] \mathrm{d}t$$

and

$$Y(\omega) = \frac{1}{2\pi} \int_{-\infty}^{\infty} y(t) \exp[-i\omega t] \mathrm{d}t \ ,$$

the cross-spectral density is given by

$$S_{xy}(\omega) = \lim_{T \to \infty} \frac{2\pi}{T} X*(\omega) Y(\omega) \ ,$$

where ω is angular frequency (Hino 1977).

We consider the total of $|\eta_{\beta\alpha}(\kappa, t)|$ for all N atoms in the system, taking average as follows:

$$\sigma(t) = \frac{1}{N} \sum_{\kappa=1}^{N} \left| \eta_{\beta\alpha}(\kappa, t) \right| \ .$$

This quantity is time-dependent, and represents the β–α_1 (or α_2) component of the mean departure of all atoms from the β-sites. The corner-linked rigid units modes may take the most important part in $\sigma(t)$: when atoms approach or depart from the β-sites in such modes, small or large $\sigma(t)$ may result, respectively. We consider the relation between $\sigma(t)$ and volume below.

The correlation between $\sigma(t)$ and time-dependent volume $V(t)$ was evaluated by cross-correlation functions,

$$C_{\sigma V}(\tau) = \langle \sigma(t) V(t + \tau) \rangle \ ,$$

where τ is a time-lag and the brackets $\langle \cdots \rangle$ indicate an average over time providing that the processes are stationary. The essential feature of $C_{\sigma V}(\tau)$ at $\tau = 0$ was essentially free from fictitious mass W. Figure 6 shows the cross-correlation functions at some selected temperatures, calculated from the Fourier transform of cross-spectral density of the two processes $S_{\sigma V}(\omega)$ by using the FFT (fast Fourier transform) program of Hino (1977), where strong negative correlation at zero time lag is seen. (As mentioned again later, the time scales of the fluctuations of volume or $\sigma(t)$ changed with the different values of the fictitious mass W). The clear negative correlation suggests that while atoms are collectively moving toward or away from the β-sites, the crystal expands or contracts, respectively. The macroscopic thermal expansion is to be contributed by these dynamical factors averaged over time or ensemble. Then we take the importance of the time-average of $\sigma(t)$ into consideration of the (macroscopic) thermal expansions. More frequent collective transfer of atoms between the α_1- and α_2-sites causes smaller $\langle \sigma(t) \rangle$, whereas increased vibrational amplitudes in the modes with the substantial rotational components of the corner-linked rigid units, which carry atoms far beyond the room-temperature α_1- or α_2-sites, cause large $\langle \sigma(t) \rangle$. In any event, we can formulate that, if the time average, $\langle \sigma(t) \rangle$, increases or decreases with varying temperature, the dynamical factors work to decrease or increase the time-averaged cell dimensions, respectively. The temperature dependence of $\langle \sigma(t) \rangle$ may reflect the result of the competition between the two factors, i.e., transfer frequency and amplitudes. As shown in Fig. 7a and b, the $\langle \sigma(t) \rangle$ value reducing from nearly 1.0 at room temperature to the

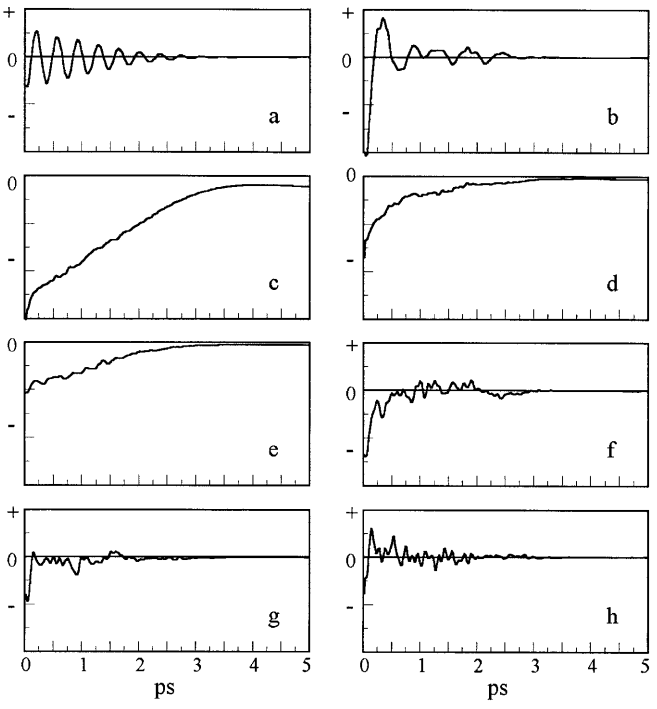

Fig. 6a–h Cross-correlation functions between $\sigma(t)$ and cell volume: **a** $\Delta T = -610$, **b** -110, **c** -10, **d** 0, **e** $+20$, **f** $+40$, **g** $+90$, **h** $+390$ K. $\sigma(t)$ is $\langle |\eta_{\beta\alpha}(\kappa, t)| \rangle$, where $\langle \ldots \rangle$ means to take the average over all atoms. Function values in vertical axes are in arbitrary scales. For **c**, **d**, and **e**, *vertical scales* are six times larger than for other temperatures

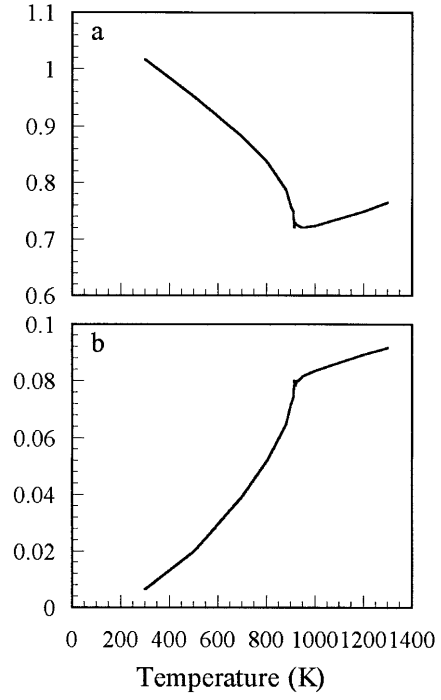

Fig. 7a, b Temperature dependence of $\langle\sigma(t)\rangle$ and transfer rates of atoms from α_1-sides to α_2-sides and vice versa. **a** $\langle\sigma(t)\rangle$ and **b** transfer rates expressed per atom and step. *Lines* connect hidden data points

minimum of about 0.73 at the transition is associated by the steep increase of transfer rate of atoms in the α-phase. This negative relation suggests that the smaller $\langle\sigma(t)\rangle$ at higher temperatures in the α-phase arises from more frequent collective transfer of atoms between the α_1- and α_2-sites. In the β-phase, the increasing trend of the transfer rate weakens (Fig. 7b), but, instead, the amplitudes of vibrations become so large that they vibrate far beyond the positions corresponding to the room-temperature α_1- or α_2-sites. As a result, $\langle\sigma(t)\rangle$ turns to an increasing trend (Fig. 7a).

Structure changes at high temperatures

Figure 8 shows the time series of the molar volume and $\sigma(t)$ at $\Delta T = -610$, -10, 0, $+10$, and $+390$ K. As suggested in Fig. 6, the negative correlation between these quantities is seen over the whole part of the time series at all temperatures in Fig. 8; that is, when $\sigma(t)$ rises, the volume falls, and vice versa. At low temperatures (Fig. 8a), molar volume and $\sigma(t)$ fluctuate along nearly constant values, e.g., about 23.43 $cm^3\ mol^{-1}$ and 1.0, respectively, at $\Delta T = -610$ K. With increasing temperature, the two time series begin to fluctuate largely with much longer time scales than at lower temperatures. The long time-scale fluctuations also correlate negatively to each other, and become more remarkable as temperature approaches the transition point (Fig. 8b, c, d). The huge negative curves in the cross-correlation functions of Fig. 6 may arise from these long time-scale fluctuations. At $\Delta T = -10$ K (Fig. 8b), the volume fluctuates around about 24.2 $cm^3\ mol^{-1}$ for longer consecutive time steps and gradually changes to larger values fluctuating at about 24.4 $cm^3\ mol^{-1}$ for shorter intervals, resulting in a time scale as long as the whole time steps in a single run of the present simulation. At $\Delta T = 0$ K (Fig. 8c), there are some parts of the consecutive time steps over 10 000 steps ($=10$ ps) where the volume changes around about 24.3 $cm^3\ mol^{-1}$, which appears to be about intermediate between the two values mentioned above. The long time-scale fluctuations fade increasingly as temperature rises to more than above $\Delta T = 0$ K. At $\Delta T = +10$ K (Fig. 8d), the volume fluctuates around the larger value of about 24.4 $cm^3\ mol^{-1}$ with small amplitudes, but the steady tendency is disturbed by the shorter duration of smaller values, which are no longer visible at $\Delta T = +90$ K. At $\Delta T = +390$ K, the volume fluctuates rapidly with small amplitudes around the larger value of about 24.4 $cm^3\ mol^{-1}$ (Fig. 8e).

The characteristic features in the fluctuations of volume near the α–β transition suggest that the MD crystal changes via a transitional state, when passing the transition point. When approaching the α–β transition from below, the transitional state first appears with alternately occurring α- and β-structures. This stage of the transitional state corresponds to that represented by Fig. 8b, where the volume is seen to change gradually between the two main values. Then the transitional state changes to a more complicated stage, where the mixed crystal of α- and β-portions begins to appear alternately with the pure β-crystal in the time series: the former corresponds to the intermediate volume of about 24.3 $cm^3\ mol^{-1}$ ($\Delta T = 0$ K, Fig. 8c). The mixed crystal of α- and β-portions no longer appears at temperatures higher than $\Delta T = 10$ K (Fig. 8d). The α-structure stands for longer time intervals than the β-structure at $\Delta T = -10$ K, but the situation is reversed at $\Delta T = 10$ K. This transitional state persists probably up to $\Delta T = +100$ K, where the typical β-phase structure with the hexagonal symmetry is attained.

The slight increase in the cell dimensions in the range of about 100 K above the transition point (Fig. 1c) can be explained in relation to the emergence of the transitional state. As temperature rises through the transition, the structure changes rather continuously via the transitional state. The cell dimensions rise continuously during these changes until the typical β-structure is attained. The top of the **c**-axis dimension appearing in Fig. 1c may correspond to the end of the transitional state. After attaining the typical β-structure, the negative contribution from large amplitudes becomes visible for the **c**-dimension, but not for the **a**-dimension. We have no atomic view at this moment of how this difference occurs.

Welche et al. (1998) and Heine et al. (1999) explained the essential feature of the thermal expansion in the quartz structure by taking a geometrical negative contribution due to the rotational modes of SiO_4 units and positive contribution from anharmonicity of the

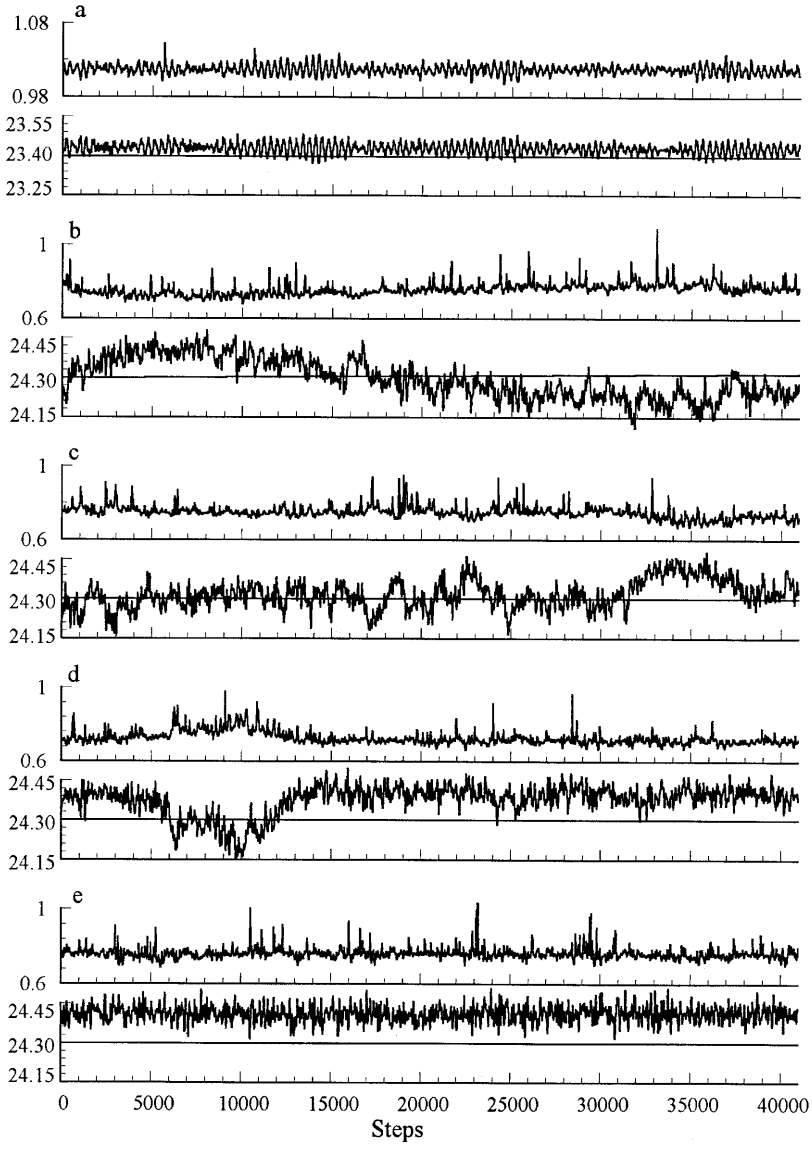

Fig. 8a–e Time series of molar volumes (*lower*) and $\langle\sigma(t)\rangle$ (*upper*) in pairs: **a** $\Delta T = -610$, **b** -10, **c** 0, **d** $+10$ and **e** $+390$ K. Molar volumes in cm^3

interatomic forces. In viewing the motions of each atom in the β-phase (Fig. 5), we also ascribe the main oscillatory component in $\sigma(t)$ to the transferring motions of atoms between the α_1- and the α_2-sites. Even in the α-phase, such transferring motions of atoms could frequently occur at high temperatures (Fig. 5b, c), but remain less oscillatory (more-random) than in the β-phase.

The mean squares volume fluctuations, $\langle(\delta V)^2\rangle$, calculated by

$$\langle\delta(V)^2\rangle = \langle(V - \langle V\rangle)^2\rangle \ ,$$

show a characteristic behavior in the vicinity of the transition point, i.e., the values gradually rise to maximum at the transition, but fall steeply in the β-phase (Fig. 9a). This behavior may also be explained in relation to the transitional state. The largely fluctuating volume in the transitional state results in larger $\langle(\delta V)^2\rangle$ than in the structure at temperatures away from the transition point. Besides the structural problems discussed, we may also calculate the bulk modulus of such a system using the equation

$$K = -V\left(\frac{\partial P}{\partial V}\right) = \frac{VkT}{\langle(\delta V)^2\rangle}$$

(Haile and Graben 1980), and compare with the experimental results to examine the accuracy of our MD volume fluctuations. Our value at $\Delta T = -610$ K ($= 300$ K) is 45.5 GPa, a little larger than the experimental value of 37.1 GPa at room temperature (McSkimin et al. 1965). The temperature evolution of our MD values is shown in Fig. 9b.

Tsuneyuki et al. (1990) found that their MD crystal of 48 hexagonal cells transformed at 850–900 K with increasing temperature, and ascribed the dynamical character of the β-phase structure to cluster dynamics. In the drawing of the trajectories of atomic positions for 4 ps, they observed locally α_1- and α_2-domains, switch-

ing to each other at 900 K. We note that these authors' simulations are done with the small MD cell at a temperature just above the transition point. We examined the typical β-phase structure in drawing the trajectories of atoms accumulated over different time intervals. Figure 10 shows the projections of the trajectories of atoms in a tetrahedron and its neighboring atoms on to the $(001)_{hex}$ planes over different intervals at $\Delta T = +390$ K. A series of trajectories accumulated over the consecutive intervals of 1 ps indicates that the atoms move well through the area centered to the β-sites in a period shorter than 1 ps, while there is no obvious sign of α_1- or α_2-domains over the period. The present observations about the atomic trajectories lead us to exclude the idea that the typical β-phase is the time average of clusters of α-quartz on time scales longer than 1 ps or even 0.5 ps. Our model of β-quartz is essentially the same as that of berlinite by Kihara and Matsui (1999), where the double-minimum feature remains, but atoms can move over the barriers in the vibrational modes, whose time scales are of the order of a few tenths of a ps. The present model of β-quartz could be compatible with most previous studies based on experiments (Tezuka et al. 1991; Salje et al. 1992; Spearing et al. 1992; and so on).

The periods of the fluctuations of the molar volume and $\sigma(t)$ were slightly different by using the different values of fictitious mass W in the NPT simulation. A larger W causes a longer period and vice versa. We may read the period of about 0.36 ps ($\approx$28 waves in 10 ps) in Fig. 8a for $W = 500$ g mol^{-1}, whereas it reduces to about 0.30 ps for $W = 100$ g mol^{-1}, both for the 1200-cell at $\Delta T = -610$ K. The time scales of the volume fluctuations or $\sigma(t)$ given in this study are fictitious.

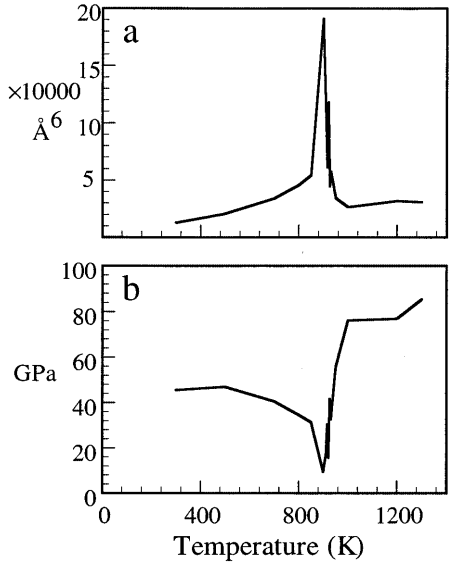

Fig. 9a, b Temperature evolution of mean-squares volume fluctuations, bulk modulus and related quantity: **a** $\langle(\delta V)^2\rangle$ for MD cell in Å^6 and **b** bulk modulus K in GPa. *Lines* connect hidden data points

Concluding remarks

In the structural studies of quartz, it is a common practice to express the structural changes in terms of the rotation of corner-linked (rigid) SiO_4 tetrahedra around $\langle 100\rangle_{hex}$. In analyzing the trajectory data of MD, however, it is not practical to handle the rotational angles, because the tetrahedra are distorted from time to time by all activated vibrational modes. Instead, time-dependent atomic displacement parameters $\eta(\kappa, t)$ and their α_1–β components $\eta_{\beta\alpha}(\kappa, t)$ were defined and used to analyze the structural changes in detail.

The present MD simulation succeeded to confirm that, with increasing temperature, the Si-O bonds in quartz expand, while the Si-O-Si angles are remarkably widened. In addition, the present study showed that thermal expansion in quartz is also related to atomic displacements, more or less, in collective transferring motions over the barriers between the α_1- and the α_2-potential-energy minima.

In the present MD crystal, the structural change from α to β occurs rather gradually via a transitional state persisting within about 100 K. The continuous structural changes in the transitional state cause the slight and continuous expansion after the steep rise of volume up to the nearly horizontal curve. During the transitional state, the hexagonal symmetry is yet to be attained.

Fig. 10a–d The trajectories of positions of atoms in an arbitrary chosen tetrahedron and of some neighboring atoms at $\Delta T = +390$ K. **a** 0.1, **b** 0.5, **c** 1, **d** 10 ps

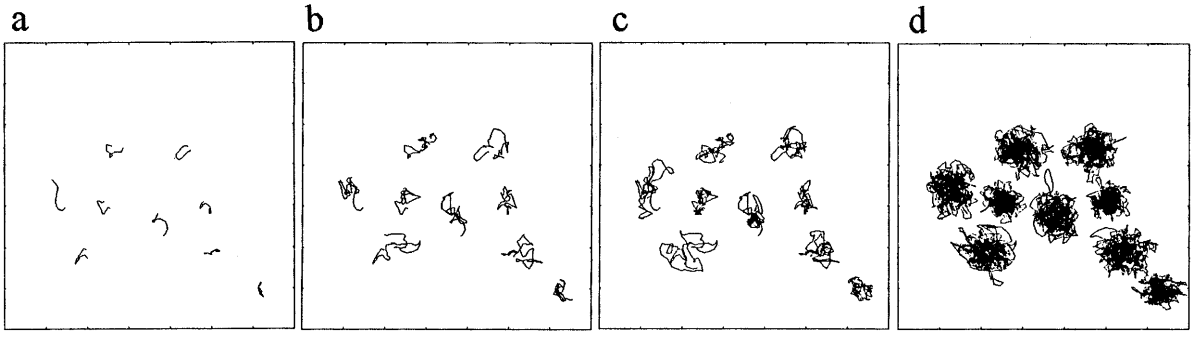

Acknowledgements The author expresses sincere thanks to Professor M. Matsui of Kyusyu University for the use of computer program CTPMD, and his valuable suggestions. Professor Subrata Ghose is to be sincerely thanked for his kind suggestions and comments. Thanks are also due to Dr. Darius Greenidge for his many comments during the preparation of the manuscript.

References

Ackermann RJ, Sorrell CA (1974) Thermal expansion and the high–low transformation in quartz. I. High-temperature X-ray studies. Acta Crystallogr 7: 461–467

Andersen HC (1980) Molecular dynamics simulations at constant pressure and/or temperature. J Chem Phys 72: 2384–2393

Carpenter MA, Salje EKH, Graeme-Barber A, Wruck B, Dove MT, Knight KS (1998) Calibration of excess thermodynamic properties and elastic constant variations associated with the $\alpha \leftrightarrow \beta$ phase transition in quartz. Am Mineral 83: 2–22

De Boer K, Jansen PJ, Santen RA van (1996) Free-energy calculations of thermodynamic, vibrational, elastic, and structural properties of α-quartz at variable pressures and temperatures. Phys Rev B 54: 826–835

Dove MT, Keen DA, Hannon AC (1997) Direct measurement of the Si-O bond length and orientational disorder in the high-temperature phase of cristobalite. Phys Chem Miner 24: 311–317

Downs RT, Gibbs GV, Bartelmehs KL, Boisen MB JR (1992) Variations of bond lengths and volumes of silicate tetrahedra with temperature. Am Mineral 77: 751–757

Grimm H, Dorner B (1975) On the mechanism of the α–β phase transformation of quartz. J Phys Chem Sol 36: 407–413

Haile JM, Graben HW (1980) On the isoenthalpic–isobaric ensemble in classical statistical mechanics. Mol Phys 40: 1433–1439

Heine V, Welche PRL, Dove MT (1999) Geometrical origin and theory of negative thermal expansion in framework structures. J Am Ceram Soc 82: 1793–1802

Hino M (1977) Spectral Analyses, in Japanese. Asakura, Tokyo

Höchli UT, Scott JF (1971) Displacement parameter, soft-mode frequency, and fluctuations in quartz below its α–β phase transition. Phys Rev Lett 26: 1627–1629

Jay AH (1933) The thermal expansion of quartz by X-ray measurements. Proc Roy Soc (A) 142: 237–247

Johnson C (1970) Generalized treatments for thermal motion. In: Willis BTM (ed) Thermal Neutron Diffraction. Clarendon Press, Oxford, pp 132–160

Kihara K (1990) An X-ray study of the temperature dependence of the quartz structure. Eur J Mineral 2: 63–77

Kihara K (1993) Lattice dynamical calculations of anisotropic temperature factors of atoms in quartz, and the structure of β-quartz. Phys Chem Miner 19: 492–501

Kihara K, Matsui M (1999) Molecular dynamics study of structural changes in berlinite. Phys Chem Miner 26: 601–614

Kosten K, Arnold H (1980) Die III-V-Analoga des SiO_2. Z Kristallogr 152: 119–133

Kramer GJ, Farragher NP, van Beest BWH, van Santen RA (1991) Interatomic force fields for silicas, aluminophosphates, and zeolites: derivation based on ab initio calculations. Phys Rev (B) 43: 5068–5080

Liebau F, Böhm H (1982) On the co-existence of structurally different regions in the low–high quartz and other displacive phase transformations. Acta Crystallogr (A) 38: 252–256

McSkimin HJ, Andreatch P, Thurston RN (1965) Elastic moduli of quartz versus hydrostatic pressure at 25° and −195.8 °C. J Appl Phys 36: 1624–1632

Megaw HD (1973) Crystal structures: a working approach. WB Saunders Company, Philadelphia, London Toronto

Miyake A, Hasegawa H, Kawamura K, Kitamura M (1998) Symmetry and its change in reciprocal space of a crystal simulated by molecular dynamics: application to quartz. Acta Crystallogr A54: 330–337

Muraoka Y, Kihara K (1997) The temperature dependence of the crystal structure of berlinite, a quartz-type form of $AlPO_4$. Phys Chem Miner 24: 243–253

Nosé S (1984) A molecular dynamics method for simulations in the canonical ensemble. Mol Phys 52: 255–268

Parrinello M, Rahman A (1981) Polymorphic transitions in single crystals: a new molecular dynamics method. J Appl Phys 52: 7182–7190

Salje EKH, Rodgwell A, Güttler B, Wruck B, Dove MT, Dolono G (1992) On the displacive character of the phase transition in quartz: a hard-mode spectroscopy study. J Phys: Cond Matter 4: 571–577

Sorrell CA, Anderson HU, Ackermann RJ (1974) Thermal expansion and the high-low transformation in quartz. II. Dilatometric studies. Acta Crystallogr 7: 468–473

Spearing DR, Farnan I, Stebbins JF (1992) Dynamics of the α–β phase transitions in quartz and cristobalite as observed by in situ high temperature ^{29}Si and ^{17}O NMR. Phys Chem Miner 19: 307–321

Tautz FS, Heine V, Dove MT, Chen X (1991) Rigid unit modes in the molecular dynamics simulation of quartz and the incommensurate phase transition. Phys Chem Miner 18: 326–336

Tezuka Y, Shin S, Ishigame M (1991) Observation of silent soft phonon in β-quartz by means of hyper-Raman scattering. Phys Rev Lett 66: 2356–2359

Tsuneyuki S, Aoki H, Tsukada M, Matsui Y (1990) Molecular-dynamics study of the α to β structural transition of quartz. Phys Rev Lett 64: 776–779

Welche PRL, Heine V, Dove MT (1998) Negative thermal expansion in beta-quartz. Phys Chem Miner 26: 63–77

Willis BTM, Pryor AW (1975) Thermal Vibrations in Crystallography. Cambridge University Press, Cambridge

Young RA (1962) Mechanism of the phase transition in quartz. Rep 2569, Air Force Office Scientific Research, Washington 25, DC